(4)

DNA-TR-87-264

PARTICLE SUBCYCLING IN PULSED-POWER SIMULATIONS

B. Goplen
R. Worl
J. Brandenburg
Mission Research Corporation
P.O. Box 542
Newington, VA 22122-0542

30 September 1987

Technical Report

CONTRACT No. DNA 001-84-C-0208

THIS WORK WAS SPONSORED BY THE DEFENSE NUCLEAR AGENCY
UNDER RDT&E RMSS CODE B323084466 T99QMXLA00013 H2590D.

Prepared for
Director
DEFENSE NUCLEAR AGENCY
Washington, DC 20305-1000

Destroy this report when it is no longer needed. Do not return to sender.

PLEASE NOTIFY THE DEFENSE NUCLEAR AGENCY, ATTN: STTI, WASHINGTON, DC 20305-1000, IF YOUR ADDRESS IS INCORRECT, IF YOU WISH IT DELETED FROM THE DISTRIBUTION LIST, OR IF THE ADDRESSEE IS NO LONGER EMPLOYED BY YOUR ORGANIZATION.

DISTRIBUTION LIST UPDATE

This mailer is provided to enable DNA to maintain current distribution lists for reports. We would appreciate your providing the requested information.

- ☐ Add the individual listed to your distribution list.
- ☐ Delete the cited organization/individual.
- ☐ Change of address.

NAME: _____

ORGANIZATION: _____

OLD ADDRESS	CURRENT ADDRESS
_____	_____
_____	_____
_____	_____

TELEPHONE NUMBER: ( ) _____

SUBJECT AREA(s) OF INTEREST:

_____	_____
_____	_____
_____	_____

DNA OR OTHER GOVERNMENT CONTRACT NUMBER: _____

CERTIFICATION OF NEED-TO-KNOW BY GOVERNMENT SPONSOR (if other than DNA):

SPONSORING ORGANIZATION: _____

CONTRACTING OFFICER OR REPRESENTATIVE: _____

SIGNATURE: _____

CUT HERE AND RETURN

Director
Defense Nuclear Agency
ATTN: TITL
Washington, DC 20305-1000

Director
Defense Nuclear Agency
ATTN: TITL
Washington, DC 20305-1000

REPORT DOCUMENTATION PAGE

1a REPORT SECURITY CLASSIFICATION UNCLASSIFIED	1b RESTRICTIVE MARKINGS
2a SECURITY CLASSIFICATION AUTHORITY N/A since Unclassified	3 DISTRIBUTION/AVAILABILITY OF REPORT Approved for public release; distribution is unlimited.
2b DECLASSIFICATION/DOWNGRADING SCHEDULE N/A since Unclassified	
4 PERFORMING ORGANIZATION REPORT NUMBER(S) MRC/WDC-R-125	5 MONITORING ORGANIZATION REPORT NUMBER(S) DNA-TR-87-264
6a NAME OF PERFORMING ORGANIZATION Mission Research Corporation 6b OFFICE SYMBOL (If applicable)	7a NAME OF MONITORING ORGANIZATION Director Defense Nuclear Agency
6c ADDRESS (City, State, and ZIP Code) P.O. Box 542 Newington, VA 22122-0542	7b ADDRESS (City, State, and ZIP Code) Washington, DC 20305-1000
8a NAME OF FUNDING/SPONSORING ORGANIZATION 8b OFFICE SYMBOL (If applicable) RAEV/Hebert	9 PROCUREMENT INSTRUMENT IDENTIFICATION NUMBER DNA 001-84-C-0208
8c ADDRESS (City, State, and ZIP Code)	10 SOURCE OF FUNDING NUMBERS PROGRAM ELEMENT NO: 62715H; PROJECT NO: T99QMXL; TASK NO: A; WORK UNIT ACCESSION NO: DH008390

11 TITLE (Include Security Classification)

PARTICLE SUBCYCLING IN PULSED-POWER SIMULATIONS

12 PERSONAL AUTHOR(S)
Goplen, Bruce; Worl, Richard; Brandenburg, John

13a TYPE OF REPORT	13b TIME COVERED	14 DATE OF REPORT (Year, Month, Day)	15 PAGE COUNT
Technical	FROM 840419 TO 870818	870930	36

16 SUPPLEMENTARY NOTATION
This work was sponsored by the Defense Nuclear Agency under RDT&E RMSS Code B323084466 T99QMXLA00013 H2590D.

17 COSATI CODES		
FIELD	GROUP	SUB-GROUP
20	8	
12	5	

18 SUBJECT TERMS (Continue on reverse if necessary and identify by block number)
Particle Subcycling; MAGIC; Pulsed-Power; Particle-in-Cell; Subcycling Cyclotron Instability

19 ABSTRACT (Continue on reverse if necessary and identify by block number)

A particle subcycling algorithm has been developed for and tested in the MAGIC code. The objective is to achieve greater efficiency in pulsed-power simulations. The algorithm performs particle kinematics calculations using a time step which is smaller than the electromagnetic time step, thereby allowing orbit resolution in regions of high magnetic field. In testing this algorithm, an energy nonconserving instability was observed. This instability, named the subcycling cyclotron instability, has been verified analytically. Its immediate effect is to diminish the utility of the particle subcycling algorithm for the intended application.

20 DISTRIBUTION/AVAILABILITY OF ABSTRACT ☐ UNCLASSIFIED/UNLIMITED ☒ SAME AS RPT ☐ DTIC USERS	21 ABSTRACT SECURITY CLASSIFICATION UNCLASSIFIED
22a NAME OF RESPONSIBLE INDIVIDUAL Sandra E. Young	22b TELEPHONE (Include Area Code) (202) 325-7042 22c OFFICE SYMBOL DNA/CSTI

DD FORM 1473, 84 MAR 83 APR edition may be used until exhausted. All other editions are obsolete.

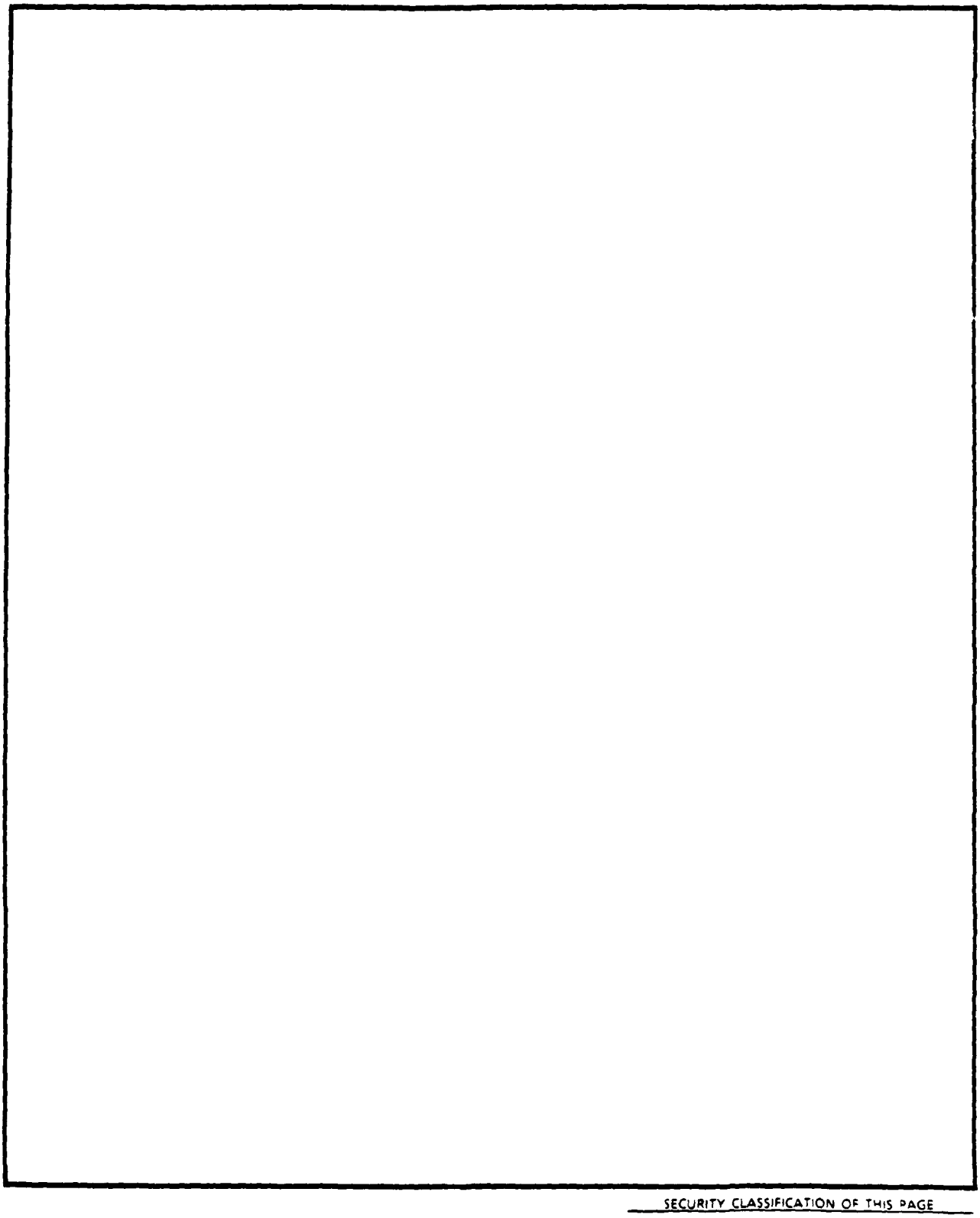

PREFACE

The authors express their appreciation to Nino Pereira of Berkeley Research Associates for suggesting the particle subcycling problem.

TABLE OF CONTENTS

LIST OF ILLUSTRATIONS

SECTION 1
INTRODUCTION

High-power diodes envisioned for the 1990s pose a significant challenge for conventional numerical simulation techniques. One problem is due to enhancement of magnetic field effects in the central, high-energy density region of the diode.

In the conventional simulation, the fundamental electromagnetic frequency (ω_f) dominates the choice of spatial grid,

$$\delta x \ll \frac{2\pi c}{\omega_f} \quad , \tag{1}$$

to achieve spatial resolution of the wavelength. Hence the Courant-limited electromagnetic time step can be related to the highest frequency by

$$\omega_f \delta t \ll 2\pi \quad . \tag{2}$$

In most regions of a pulsed-power system, the cyclotron frequency,

$$\omega_c \delta t = \frac{eB\delta t}{m} \quad , \tag{3}$$

presents a less restrictive constraint. That is, a conventional particle kinematics algorithm can usually resolve the orbital motion using a time step dictated by electromagnetic wave requirements. However, due to field compression and charge leakage, the magnetic field in the central region of a diode can be sufficiently large that orbital motion is not resolved. Section 2 of this report will demonstrate this effect upon calculated particle trajectories.

To address this problem, a particle subcycling algorithm was developed and implemented in MAGIC[†]. The basic idea of subcycling is to integrate the electron trajectories using a time step smaller than the electromagnetic time step, thus permitting trajectory resolution without an excessive number of electromagnetic calculations. To test variations, the new algorithm in MAGIC contained five options implemented in a new executive module. These options and the executive module are described in Section 3.

Tests of the algorithm were performed on a diode simulation problem based on Blackjack 5. These tests included a detailed analysis of computational time broken down by subroutines. These tests demonstrated that subcycling did yield an advantage in computational speed. However, tests also revealed the presence of numerical instability whenever the speed advantage became significant. Upon investigation, we were able to show theoretically and in simulations that subcycling produces instability under the conditions,

$$\omega_p/\omega_c < 1 \quad \text{and} \quad \delta t\omega_c > \pi/8 \ , \tag{4}$$

where ω_p is the plasma frequency and ω_c is the cyclotron frequency. One distinguishing feature of this instability, termed the subcycling cyclotron (SC) instability, is a nonphysical growth in energy. The subcycling cyclotron instability is discussed in Section 4 of this report.

In summary, our present belief is that subcycling will not be useful for pulsed-power applications. However, in other plasma physics applications, it might result in a factor of two or more computational efficiency. To achieve such results, it may be necessary to subcycle electrons, while retaining a larger time step for the more massive ions.

[†]B. Goplen, R. Clark, J. McDonald, G. Warren, and R. Worl, "MAGIC User's Manual," Mission Research Corporation Report, MRC/WDC-R-126, April 1987.

SECTION 2
SINGLE PARTICLE ORBITS

2.1 PROBLEM DESCRIPTION.

The problem of simulating self-consistent particle motion in regions of high magnetic field has two related aspects. First, the conventional kinematics algorithms will not correctly compute the particle orbit if the time step is too large. Thus, the basically circular motion inherent in physical drifts (ExB, Bx∇B, etc.) will not be correctly resolved. Second, charge- and current-density contributions from the particle orbit will not be correctly resolved if the spatial grid is too large.

These two apsects are, of course, related. For example, if the spatial grid is sufficiently small to represent charge and current densities correctly, then the time step (Courant limited by the spatial grid) would be small enough to resolve the particle orbit. However, the computational expense associated with such a brute-source approach is prohibitive. Thus, the desire is to treat the particles in some special way (e.g., guiding center, subcycling, etc.) to avoid the small spatial grid and time step.

To demonstrate the problem graphically, we present the results of single particle orbits calculated with the MAGIC kinematics algorithm using different time steps, i.e., $\tau/10$, $\tau/4$, ...

2.2 CONVENTIONAL KINEMATICS ALGORITHM.

The kinematics algorithm in MAGIC was originally developed by Boris[†]. Here, we discuss only that aspect which relates to the magnetic field term. Physically, the equation of motion,

$$\frac{d\bar{p}}{dt} = -\frac{e}{m}\ \bar{v} \times \bar{B} \quad , \tag{5}$$

[†]J. P. Boris, Relativistic Plasma Simulation--Optimization of a Hybrid Code, Proceedings of the Fourth Conference on Numerical Simulation of Plasmas, Naval Research Laboratory (1970), p. 3.

should result in a rotation in the plane transverse to B through an angle,

$$\beta = \frac{-e\delta t\ B}{\gamma m} \ , \tag{6}$$

without change in the magnitude of the momentum vector. The procedure for calculating the rotation in MAGIC is illustrated in Figure 1. First, an intermediate momentum vector is calculated from the vector addition,

$$\bar{p}_b = \bar{p}_a + f_1 \bar{p}_a \times \bar{B} \ , \tag{7}$$

where

$$f_1 = \frac{\tan \dfrac{-e\delta t \left|\bar{B}\right|}{2\gamma m}}{\left|\bar{B}\right|} \ . \tag{8}$$

In MAGIC, use is made of the expansion,

$$\tan \beta/2 \approx \beta/2 + 0.31755(\beta/2)^3 + 0.2033(\beta/2)^5, \tag{9}$$

to calculate the geometrical factor, f_1. Finally, the rotation is completed with the calculation,

$$\bar{p}_c = \bar{p}_a + f_2 \bar{p}_b \times \bar{B} \ , \tag{10}$$

where

$$f_2 = \frac{2f_1}{1 + f_1^2 \left|\bar{B}\right|^2} \ . \tag{11}$$

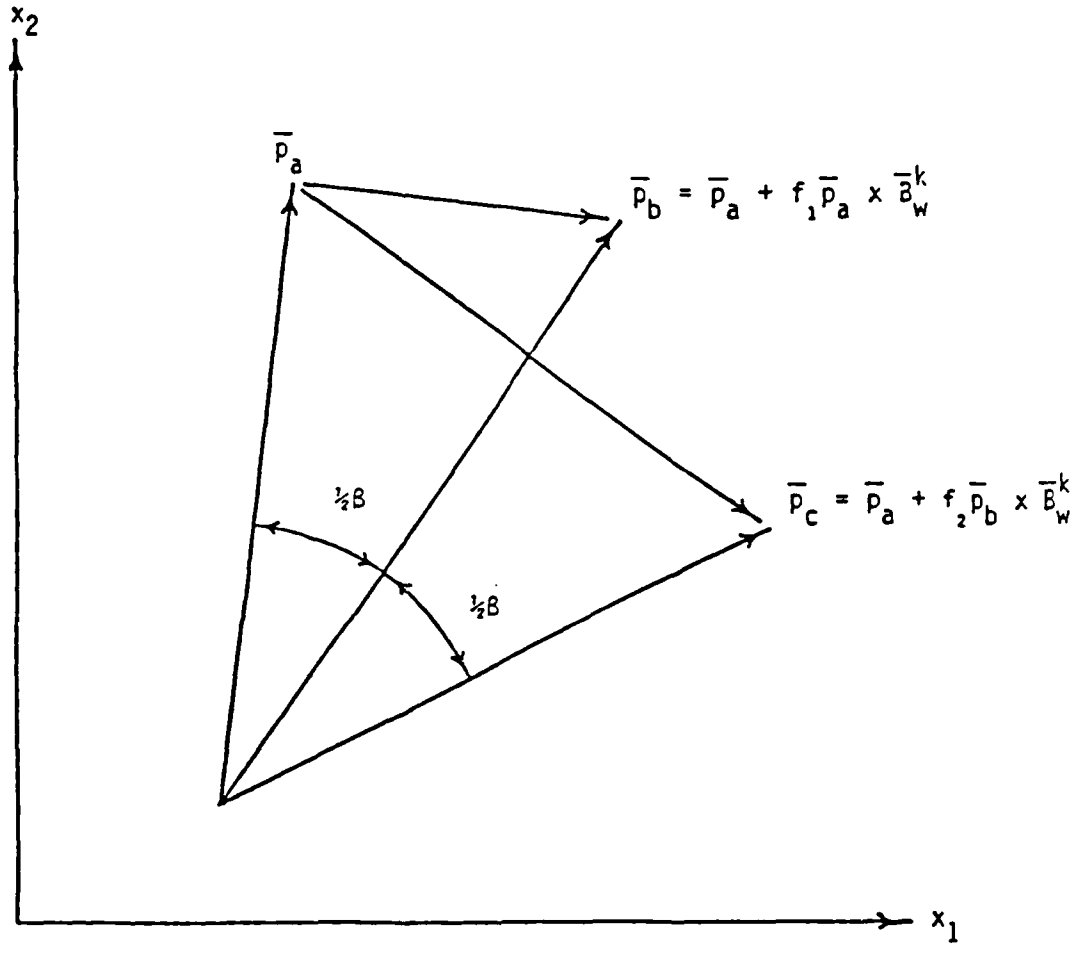

Figure 1. Particle rotation due to magnetic field.

2.3 CALCULATED ORBITS.

From the relations above, it is easy to derive calculated particle trajectories for certain pathological cases, e.g., $\delta t = \tau$, where τ is the Larmor period. However, to demonstrate this visually, we have exercised MAGIC using the POPULATE and PRESET commands to obtain trajectory plots of calculated single particle orbits. The test problem involves a 1 MeV electron in a constant magnetic field, B = 20T. The theoretical radius of gyration and Larmor period are

$$r = \frac{\gamma m v}{eB} = 2.56 \times 10^{-4} m$$

and (12)

$$\tau = \frac{2\pi\gamma m}{eB} = 5.65 \times 10^{-12} sec,$$

respectively.

Figure 2 illustrates particle trajectory plots computed using six different values of the time step, δt. Note that Figure 2a, with $\omega_c \delta t = 2\pi/100$, appears to be a perfect circular orbit. For more useful time steps, i.e., $\omega_c \delta t = 2\pi/10$ or $2\pi/4$, regular geometric figures are produced in which the number of sides is equal to the time step denominator (see Figure 2b and c). For still larger values of time step, the orbit degenerates into a straight line; i.e., the particle simply oscillates back and forth. The apparent oscillation frequency is inversely proportional to the time step, δt, and is unrelated to the Larmor period. Clearly, this is a poor representation of the physical orbit.

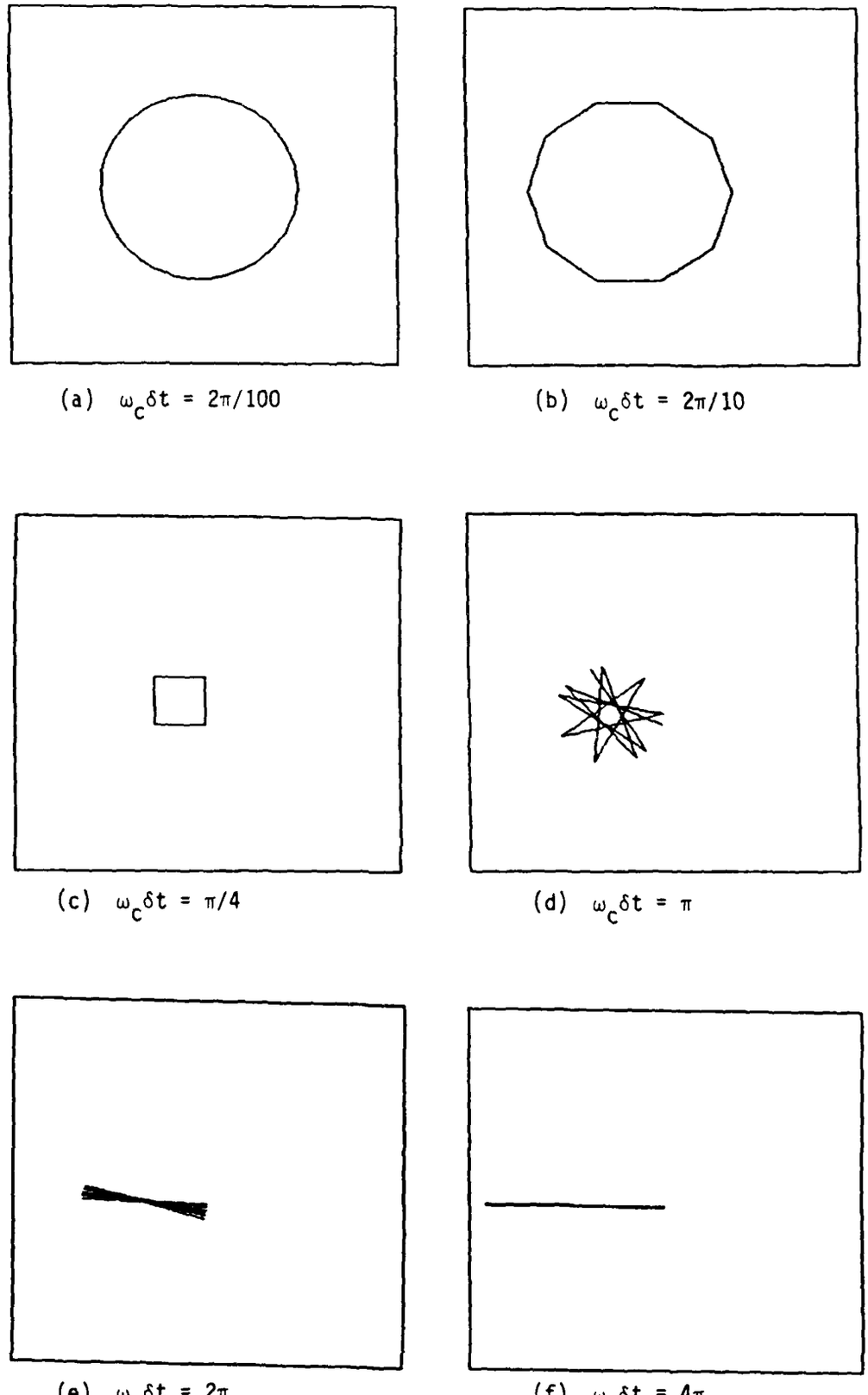

Figure 2. Calculated particle orbit vs. time step.

SECTION 3
SUBCYCLING ALGORITHM IN MAGIC

3.1 SUBCYCLING OPTIONS.

The basic idea behind particle subcycling is that the particle kinematics uses a reduced time step; i.e., one smaller than the electromagnetic time step. Of course, there are many possible variations in a subcycling algorithm; e.g., whether to use the same kinematical forces throughout the subcycle, whether to treat electrons separately from ions, and so forth. To test the effect of such variations, the algorithm implemented in MAGIC contained the options listed below. (The flag, iscopt, is an input data flag set by the user in the KINEMATICS command.)

iscopt	Subcycle Option
0	no subcycles
1	retain initial forces and final currents
2	subcycle forces and retain final currents
3	retain initial forces and subcycle currents
4	subcycle both forces and currents

3.2 FLOW DIAGRAMS.

An overview of the particle processing section of CONTROL is presented in Figure 3. First a check is done for particle creation surfaces (NCRE). If particle creation has been requested, then a flag (LSFP) is checked to ascertain whether the particle groups should be processed in this time step. If so, then a check is made (NPRS) for whether analytically determined forces are to be used to move particles. If not, then the average value of the electromagnetic fields at the full grid points is calculated by AFIELDS. Next, the particle creation is performed in CREATOR. A test is performed for the existence of particle

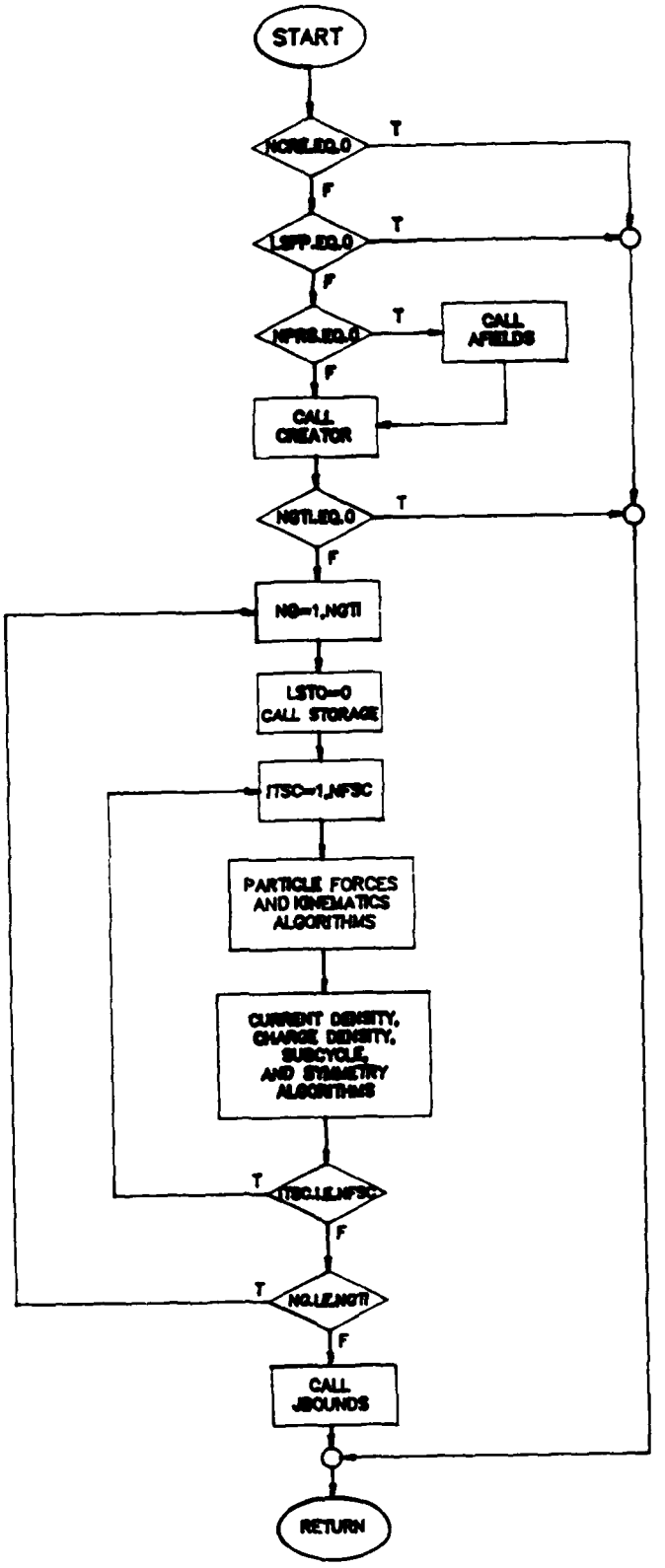

Figure 3. Executive module for particles.

groups (NGTI). Particles in MAGIC are processed in groups of 192 particles. A call is made to STORAGE for the next particle group to be processed. A loop over particle subcycles has been placed inside of the loop over particle groups. The particle kinematics time step is determined by dividing the electromagnetic time step by the subcycle frequency (NFSC).

Figure 4 is a flow diagram showing how the subcycle options have been implemented for particle forces and kinematics. A test on the subcycle option flag (LFSC) and the subcycle loop counter (ITSC) is made to determine if particle forces are to be subcycled. When LFSC=1 or LFSC=3 and ITSC is greater than 1, then the calls to the subroutines, PREDICT which calculates the electromagnetic forces at the particle position, or PRSCRIB, which determines analytical values for the electromagnetic forces, are calculated for the first subcycle and bypassed for subsequent subcycles.

For LFSC=2 and LFSC=4, the forces are calculated for every subcycle. The corrector flag (LCOR) is initialized next. The subroutines, KINEMAT, which computes particle trajectories, and ROTATOR, which transforms particle coordinates and momenta, are called for every subcycle. If the predictor flag has been set (LPRE=1), then the corrector flag is set (LCOR=1) and CORRECT, which corrects the electromagnetic forces for the new particle positions through a modified Euler method, or PRSCRIB, which computes analytical forces, is called and KINEMAT and ROTATOR are called again. After the particle trajectories have been computed, then, if requested, the trajectories are written to a file for plotting by TRAJECT.

Figure 5 is a flow diagram showing how the subcycle options have been implemented for current density calculations. When the particle kinematics are completed, the subcycle option flag is evaluated. If LFSC=1 or LFSC=2, then SUBCYCL is called, which for these options saves the initial particle coordinates and momenta of the first subcycle for calculation of the current density on the last subcycle. The weighting

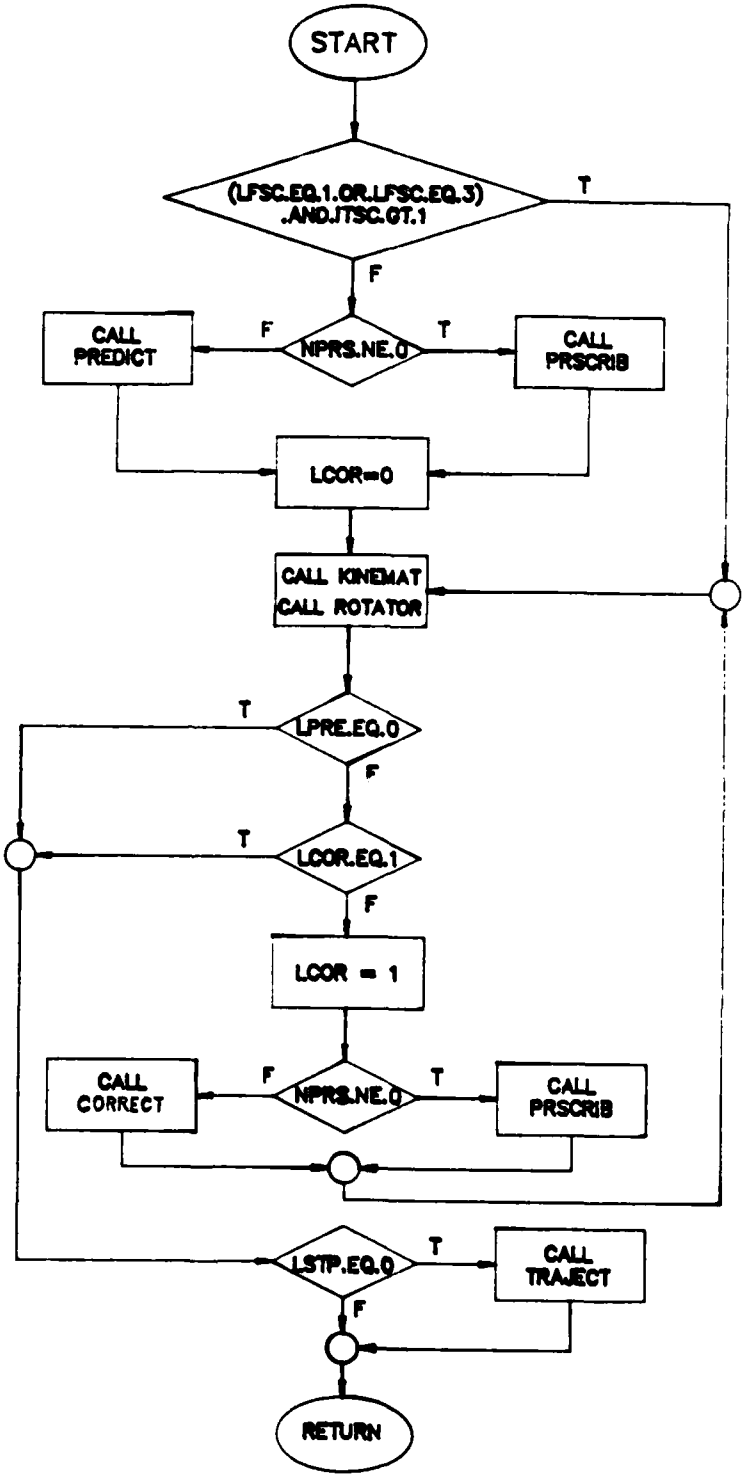

Figure 4. Particle forces and kinematics algorithms.

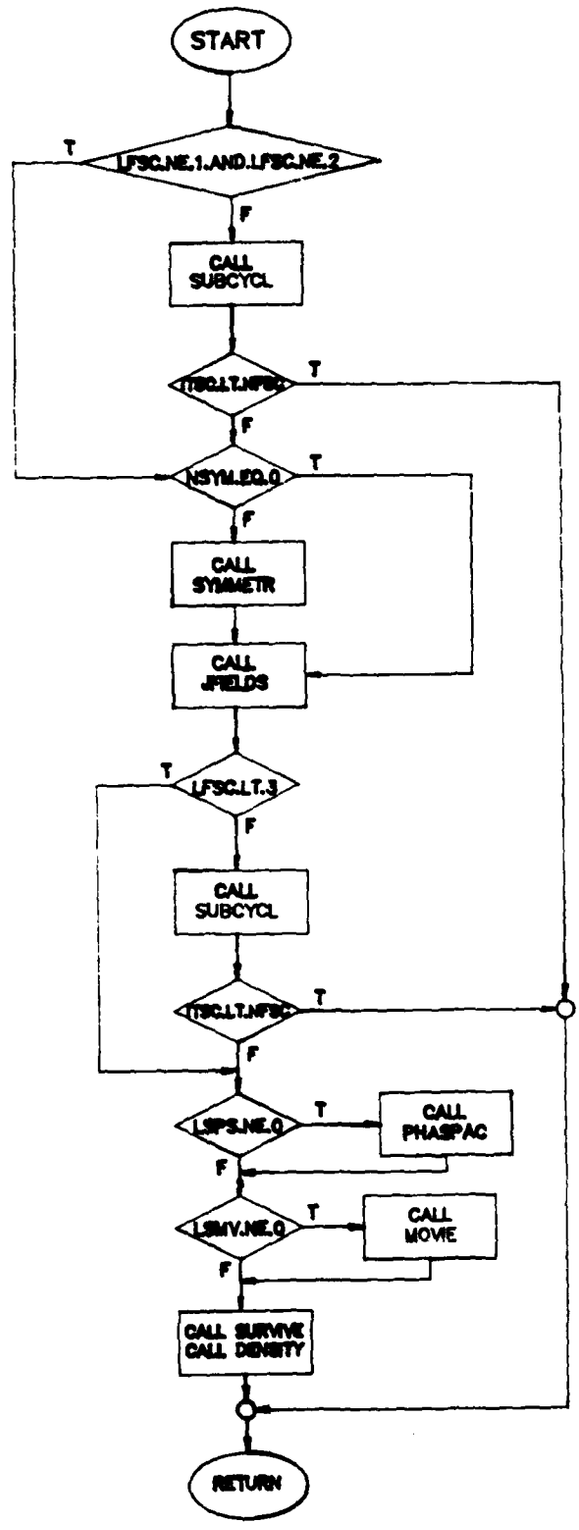

Figure 5. Current density, charge density, subcycle, and symmetry algorithms.

fractions for current density for the initial coordinates and momenta are recalculated in SUBCYCL for LFSC=2, because the subcycling of particle forces has overwritten the information. The initial particle data is replaced by the final particle data, and the program control goes to the end of the subcycle loop until the last subcycle. If LFSC=3 or LFSC=4, the current density is calculated for every subcycle. First, any symmetry boundaries are accounted for in SYMMETR, and then the current density is calculated in JFIELDS. A call to SUBCYCL is made after JFIELDS to swap final particle data for initial particle data and to calculate current density weighting fractions for LFSC=3, since particle forces are not computed every subcycle. CONTROL then branches to the end of the loop until the last subcycle, where particle data is written to disk for phase space and movie plotting by subroutines PHASPAC and MOVIE, if requested. Killed particles are accounted for in SURVIVE and charge density at full grid points is computed in DENSITY.

When the subcycle loop and the particle group are completed, then JBOUNDS takes care of the effects of boundary conditions on current density.

3.3 KINEMATICS COMMAND.

Function: Specifies the particle kinematics algorithm.

Format:

KINEMATICS itmult irel apcopt a3dopt iscopt nfsc /

Arguments:

itmult - Particle-to-field time step ratio (integer).
irel - Relativistic flag (integer)
apcopt - Predictor-corrector option (alpha).
= YES or NO.
a3dopt - Three-dimensional option (alpha).
= YES or NO.

iscopt - Particle subcycle option (integer).

= 0, no subcycle (default).

= 1, retain initial forces and final currents.

= 2, subcycle forces and retain final currents.

= 3, retain initial forces and subcycle currents.

= 4, subcycle both forces and currents.

nfsc - Subcycle frequency (integer).

= 1, (default).

Description:

The KINEMATICS command is used to specify the particle algorithm. The particle-to-field time step ratio determines whether particle kinematic calculations are performed for every field calculation or some multiple of the field calculation. Only relativistic kinematics are presently available in MAGIC: the relativistic flag input is simply ignored by the code. The predictor-corrector option can be used to estimate forces on a particle throughout the duration of the time step. It recalculates the particle trajectory based on that correction. This requires two cycles through the kinematics algorithm and is therefore more expensive. The full three-dimensional kinematics option is usually selected, but the simpler two-dimensional kinematics can be used when the TE mode is not present or when motion in the third dimension is not relevant.

The particle subcycle option enables the particle kinematics calculation to be performed in a multiple of steps or subcycles for each calculation of the fields. The options include no subcycling of the kinematics (which is the default), subcycling only the particle trajectory calculations, subcycling the weighted forces at particle position along with the particle trajectories, subcycling the current density calculation along with the trajectories, subcycling the forces and the current density along with the particle forces.

SECTION 4
SUBCYCLING CYCLOTRON INSTABILITY

4.1 OVERVIEW.

This section analyzes an instability we have termed the Subcycling Cyclotron (SC) instability. The analysis is restricted in its validity to systems in which

$$\omega_c/\omega_p > 1 \quad , \tag{13}$$

where ω_p and ω_c are the electron plasma and cyclotron frequencies, respectively. It can be shown, however, that this condition will occur in many systems for which subcycling would otherwise be useful. The SC instability is therefore a serious problem and, if methods cannot be found to eliminate it, this may seriously limit the utility of subcycling in simulations.

A derivation of the SC instability will be done using the fluid theory of cyclotron waves. It will be shown that for the conditions of Equation (13) and the limit of exact equations of motion and fields, that only stable electron cyclotron waves will result. The electric fields due to charge fluctuations will be only a perturbation on the electron motion, and the wave frequency will be nearly the cyclotron frequency.

In the case of subcycling, however, the perturbing electric field will no longer lead to a stable wave. The effect of subcycling will lead to an effective "phase lag" of the electrostatic perturbation on the electron orbit. This phase lag will lead to a growing amplitude of the electric fields and the electron energy. This instability will be fastest growing for the condition,

$$\omega_c \delta t = \pi \quad , \tag{14}$$

where δt is the electromagnetic time step. The SC instability will be clearly distinguishable from a physical instability in that it will lead to a growth in

total system energy. A physical instability, conversely, will conserve total energy, merely transforming it from one degree of freedom to another. Therefore, the instability will then lead to an unphysical heating of electrons and a deterioration of energy balance in simulations employing subcycling.

The results of simulations confirming the basic features of the analytic theory will be shown. These simulations were performed for charge neutral systems but are fully relevant to the non-neutral case. The simulations show a growing instability in the system associated with the degree of subcycling.

4.2 FLUID THEORY OF CYCLOTRON WAVES.

We will use the fluid description of the electrons found in a text by Chen[†]. Following this treatment, we can derive the equations governing electron cyclotron waves in a cold (monoenergetic) electron plasma with a neutralizing ion background.

We begin with the linearized equations for motion, continuity, and electric field, respectively. These are

$$m\partial_t \bar{V}_1 = -e(\bar{V}_1 \times \bar{B}_0 + \bar{E}_1) \quad ,$$

$$\partial_t n_1 = -n_0 \mathrm{Div}(\bar{V}_1) \quad , \tag{15}$$

and $$\bar{E}_1 = -4\pi\, e n_1 \quad ,$$

where E_1, n_1, and V_1 are the first order perturbed electric field, electron density, and electron velocity respectively, and V_0, B_0, and n_0 are the steady-state velocity, magnetic field, and electron density, respectively. We assumed perturbations of the form, exp (kx-ωt). We break the equation of motion up into its components,

[†]Francis F. Chen, Introduction to Plasma Physics, Plenum Press (1974), p 90.

$$-i\omega m V_x = -eE - eV_y B_0 \quad ,$$

$$-i\omega m V_y = -eV_x B_0 \quad , \tag{16}$$

and $$-i\omega m V_z = 0 \quad .$$

We solve this system for V_x to obtain

$$-i\omega m V_x = eE_x + eB_0 \frac{ieB_0}{m\omega} V_x \quad , \tag{17}$$

which becomes

$$\left(1 - \frac{\omega_c^2}{\omega^2}\right) V_x = i \frac{eE_x}{m\omega} \quad , \tag{18}$$

where ω_c is the electron cyclotron frequency. We can now solve for E_x in terms of V_x to close the system. We have from the continuity equation,

$$-i\omega n_1 = in_0 k V_x \quad . \tag{19}$$

which becomes

$$n_1 = \frac{n_0 k V_x}{\omega} \quad . \tag{20}$$

We then use Poisson's equation to write

$$E_x = \frac{-4\pi e n_1}{ik} \quad , \tag{21}$$

which then becomes

$$E_x = \frac{-4\pi e n_0 V_x}{i\omega} \quad . \tag{22}$$

This expression is inserted back into Equation (18) to yield

$$\left(1-\frac{\omega_c^2}{\omega^2}\right)V_x = \frac{\omega_p^2}{\omega^2}\ V_x, \tag{23}$$

where $\omega_p^2 = 4\pi e^2 n_0/m$ and ω_p is the electron plasma frequency. This gives a dispersion relation for cold electron cyclotron waves,

$$\omega^2 = \omega_c^2 + \omega_p^2 \quad . \tag{24}$$

The frequency for these waves is real and therefore the waves are stable. For the case $\omega_p^2/\omega_c^2 \ll 1$, we find that the waves occur at nearly the cyclotron frequency,

$$\omega \simeq \omega_c \left(1+\frac{1}{2}\ \frac{\omega_p^2}{\omega_c^2}\ \right) \quad . \tag{25}$$

4.3 INSTABILITY DUE TO SUBCYCLING.

We have shown that the cyclotron motion of electrons in a plasma could lead to stable electrostatic oscillations and that, in the limit $\omega_p^2/\omega_c^2 \ll 1$, these waves have a frequency nearly that of the electron cyclotron frequency. We now consider what will happen when the particle equations of motion are advanced with a time step much shorter than the electromagnetic time step. Defining a parameter,

$$S_e = \omega_c \delta t \quad , \tag{26}$$

we will show that subcycling will perturb the cyclotron waves and cause them to become unstable, with a growth rate depending on S_e. The instability will occur because the electrostatic field develops an effective "phase lag" relative to the particle velocity.

The phase lag occurs because the electromagnetic time step defines a period over which the electric field due to charge fluctuations will be frozen in time. Thus an electron experiences fields due to the charge distributions existing at the end of the last time step rather than the instantaneous charge distribution. For a sinusoidal electric field, this can be approximated, for a small enough time step, as a phase lag. This is shown graphically in Figure 6. Therefore, for $0<S_e<2\pi$, the onset of subcycling, we can approximate the phase lag as a phase factor,

$$P_e = e^{iS_e/2} \quad . \tag{27}$$

This approximation is based on the relationships illustrated in Figure 6. The phase factor can be multiplied times the electric field from Equation 18, to yield

$$\left(1 - \frac{\omega_c^2}{\omega^2}\right) V_x = \frac{ieE}{m\omega} \; e^{iS_e/2} \quad . \tag{28}$$

The electric field is found from Equation 22. However, because the electron velocity itself is advanced in discretized steps, the electron magnetic force will experience a phase lag of

$$P_m = e^{iS_m/2} \quad , \tag{29}$$

where $P_m = \omega_c \delta t_p$ with δt_p being the time step for advancing particle motion. This phase lag for magnetic forces occurs because the Lorentz force on the electrons depends on their velocity. The velocity used to calculate magnetic forces is (in the absence of predictor-corrector algorithms) the velocity found at the end of the previous time step. From Section 2, we have demonstrated useful values of this phase lag to lie in the range,

$$0<S_m<\pi/4 \quad . \tag{30}$$

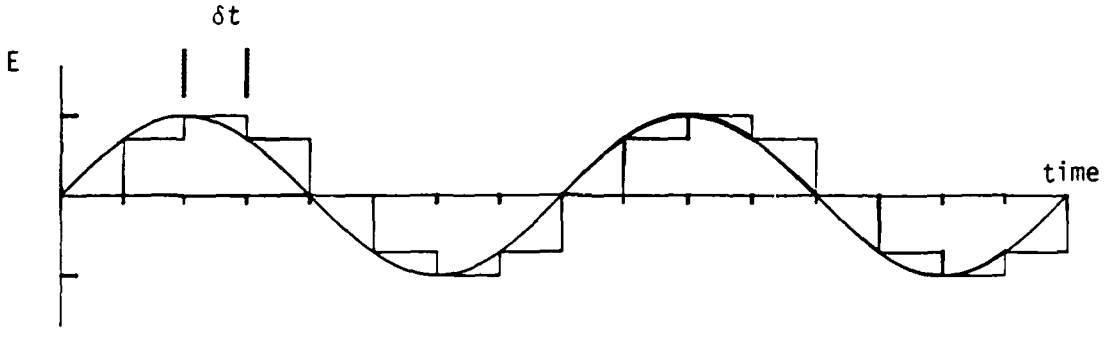

(a) Approximation of physical field over interval δt

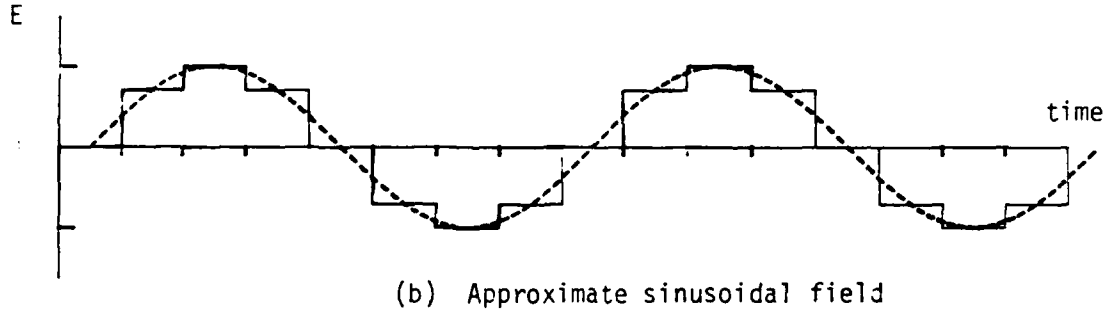

(b) Approximate sinusoidal field

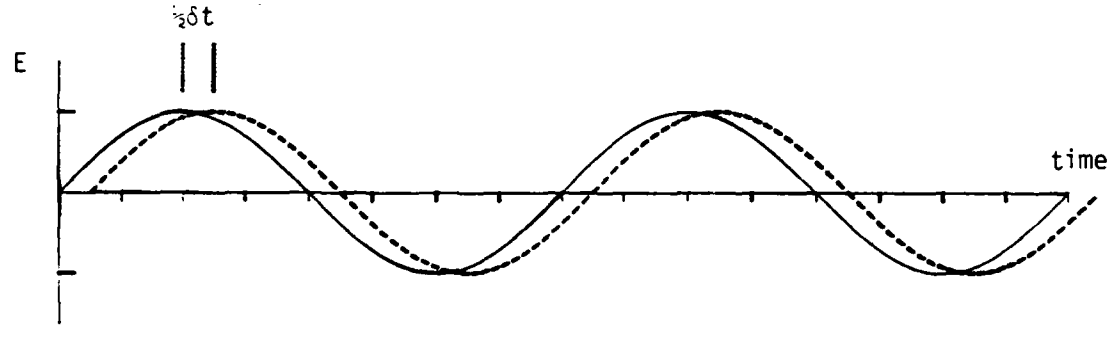

(c) Physical and approximate sinusoidal fields

Figure 6. Electric fields vs. time.

Equation 28 then becomes

$$\left(1-\frac{\omega_c^2}{\omega^2}\right) V_x e^{iS_m/2} = \frac{ieE}{m\omega} e^{iS_e/2}. \tag{31}$$

This phase lag effect due to discrete time steps does not affect the calculation of particle locations based on their velocities, which is done more accurately. The result of phase lags in magnetic and electric fields but not in charge densities is that Equation 25 is unchanged. We now have for the electron equation of motion,

$$\left(1-\frac{\omega_c^2}{\omega^2}\right) V_x e^{iS_m/2} = \frac{\omega_p^2}{\omega^2} V_x e^{iS_e/2} . \tag{32}$$

This yields a dispersion relation,

$$\omega^2 = \omega_c^2 \left(1+\frac{\omega_p^2}{\omega_c^2} e^{i(S_e-S_m)/2}\right) . \tag{33}$$

In the case of $S_m = S_e$ (no subcycling), we have

$$\omega^2 = \omega_c^2 \left(1 + \frac{\omega_p^2}{\omega_c^2}\right) . \tag{34}$$

In this case, ω is real, indicating stable waves. The parameter S_m is usually fixed at a value of $\pi/4$. For $S_e > S_m$ we have

$$\omega^2 = \omega_c^2\left(1+\frac{\omega_p^2}{\omega_c^2} e^{i(S_e/2 - \pi/8)}\right) . \tag{35}$$

The frequency is now complex,

$$\omega^2 = \omega^2 \left\{1 + \frac{\omega_p^2}{\omega_c^2} \left[\cos(S_e/2 - \pi/8) + i \sin (S_e/2 - \pi/8)\right]\right\}. \tag{36}$$

The case of most interest, $\omega_p^2/\omega_c^2 \ll 1$, yields

$$\omega \simeq \omega_c \left\{1 + \frac{1}{2} \frac{\omega_p^2}{\omega_c^2} \left[\cos(S_e/2 - \pi/8) + i \sin(S_e/2 - \pi/8)\right]\right\} . \qquad (37)$$

The imaginary part of the frequency is the growth rate and has the value

$$\text{Im}(\omega) = \frac{1}{2} \frac{\omega_p^2}{\omega_c} \sin(S_e/2 - \pi/8) . \qquad (38)$$

This formula for the SC instability growth rate is an approximation valid only for $0 < S_e < 2\pi$. However, we can test the scaling by simulation. The scaling predicts stability for $S_e = \pi/4$ and instability for $S_e > \pi/4$. A peak of instability should be reached at $S_e = 5\pi/4$ with a decrease thereafter.

4.4 SIMULATION RESULTS.

To test the theoretical model of the SC instability, several simulations were run with differing values of S_e. The simulations consisted of a charge neutral plasma of electrons and ions with a number density of $n = 10^{10}/m^3$ in a magnetic field of 0.5 Tesla. The electrons were all given the initial random speed of 2.7×10^8 m/sec. This gives a ratio of plasma frequency to cyclotron frequency, $\omega_p^2/\omega_c^2 = 10^{-2}$. The problem was run for a time of 10^{-10} seconds or roughly 100 cyclotron periods.

The distinguishing feature of the instability, which differentiates it from a physical instability at the same frequency, is the fact that energy is not conserved. In a physical instability, particles give up energy to a wave field so that energy changes form but is globally conserved. In the SC instability, both particles and wave fields gain energy at the same time, so that energy is not globally conserved but instead grows.

In Figure 7, the instability is seen in terms of global energy growth. The total system energy in fields and particles is plotted versus time. The stable case, $S_e = \pi/4$, shows a flat, straight curve of energy versus time, indicating no energy growth. In the very unstable case, $S_e = \pi/2$, Figure 7 shows that the total system energy grows rapidly, violating

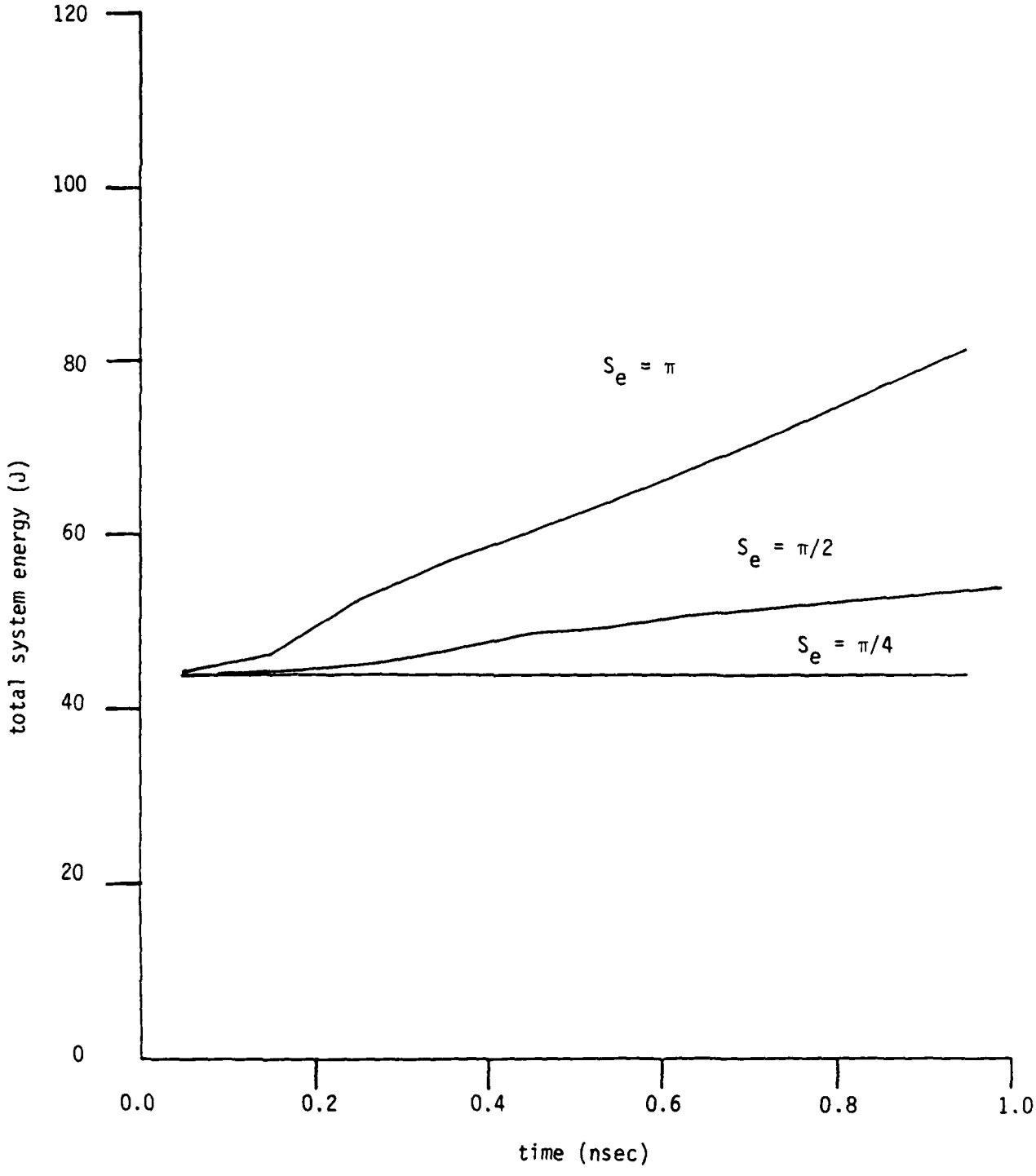

Figure 7. Total system energy vs. time.

energy conservation. The slopes of the energy versus time curves in Figure 7 are proportional to the growth rates of the SC instability. The energy growth rates for early time, when linear theory is valid, are shown in Figure 8. As can be seen, the peak growth rate is in the neighborhood of $S_e = \pi$.

The behavior at late time shown in Figure 7 indicates that some nonlinear effects occur to slow down the growth rate. These effects occur when the wave fields are no longer a small pertubation on the particle motion but begin to dominate it. Trapping of particles in the wave fields is a physical effect which can occur to slow the growth of waves.

4.5 DISCUSSION.

It has been shown theoretically and demonstrated with simulations that subcycling will lead to an instability for the case, $\omega_p^2/\omega_c^2 \ll 1$. This instability will lead to unphysical growth of both particle and wave energies. The loss of energy conservation in simulations is then one sign of SC instability. The regime in which the SC instability was demonstrated is a restricted one, corresponding to finite densities and weak subcycling. However, as has been discussed in Section 1, subcycling is only useful in cases where $\omega_c \delta t > 1$. For the problem of interest, a high current diode with regions of magnetic insulated sheaths, we will have the condition

$$\omega_p \simeq \omega_c \, . \tag{39}$$

However, in those regions, subcycling cannot be implemented without loss of accurate particle dynamics. This is due to the requirement,

$$\omega_p \delta t \quad < 1, \tag{40}$$

which must hold if the dynamics of particles in electrostatic fields is to be simulated accurately. If $\omega_p \simeq \omega_c$, then subcycling, which requires $\omega_c \delta t > 1$, cannot be in effect. The only regime of accurate electrostatic particle dynamics and useful subcycling is therefore

$$\frac{\omega_c \delta t}{\omega_p \delta t} = \frac{\omega_c}{\omega_p} > 1, \tag{41}$$

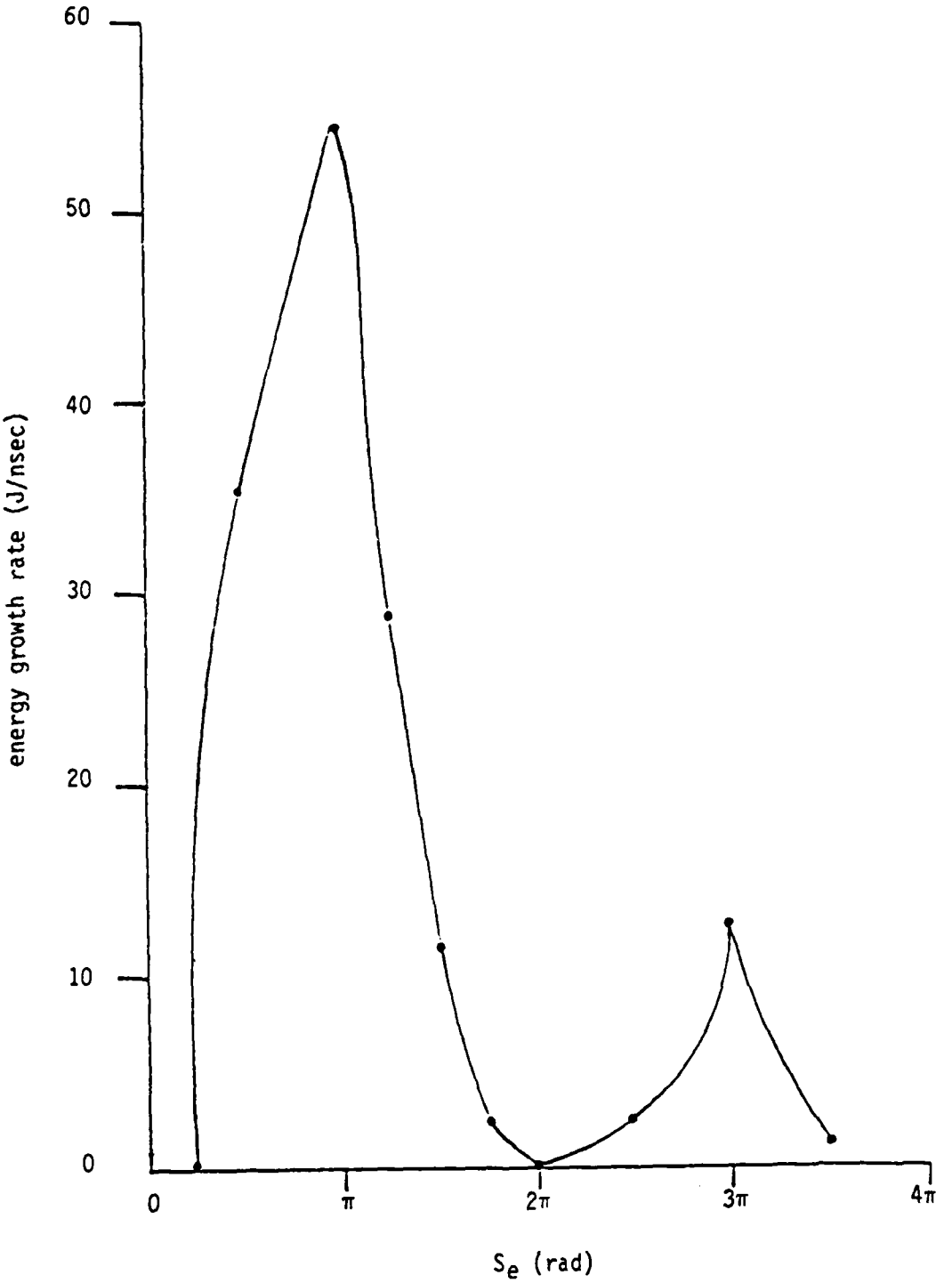

Figure 8. Growth rate of total system energy.

which is the region of SC instability. Such regions will occur outside the sheath regions of the problem. Therefore, at least for magnetically insulated systems, the only regions where subcycling would be useful are those for which it is unstable.

DISTRIBUTION LIST

(This List Is Unclassified)

DEPARTMENT OF DEFENSE

ASSISTANT TO THE SECRETARY OF DEFENSE
ATOMIC ENERGY
ATTN: EXECUTIVE ASSISTANT

DEFENSE INTELLIGENCE AGENCY
ATTN: DT-2
2 CYS ATTN: RTS-2B
ATTN: VP-TPO

DEFENSE NUCLEAR AGENCY
2 CYS ATTN: SPSD
ATTN: TDTR
4 CYS ATTN: TITL

DEFENSE NUCLEAR AGENCY
ATTN: TDNV

DEFENSE NUCLEAR AGENCY
ATTN: TDNM-CF
ATTN: W SUMMA

DEFENSE TECHNICAL INFO CENTER
12CYS ATTN: DD

DEPARTMENT OF DEF EXPLO SAFETY BD
ATTN: CHAIRMAN

JOINT STRAT TGT PLANNING STAFF
ATTN: JKAD
ATTN: JLWT
ATTN: JPEP

LAWRENCE LIVERMORE NATIONAL LAB
ATTN: DNA-LL

DEPARTMENT OF THE ARMY

U S ARMY BALLISTIC RESEARCH LAB
ATTN: SLCBR-SS-T
ATTN: B R RALEY

U S ARMY CORPS OF ENGINEERS
ATTN: DAEN-RDL

U S ARMY MATERIAL TECH LABORATORY
ATTN: TECHNICAL LIBRARY

U S ARMY MISSILE COMMAND
ATTN: AMSMI-RD-CS-R (DOCS)

U S ARMY NUCLEAR & CHEM AGENCY
ATTN: MONA-NU
ATTN: J KELLEY

USA SURVIVABILITY MANAGMENT OFFICE
ATTN: J BRAND

DEPARTMENT OF THE NAVY

DAVID TAYLOR NAVAL SHIP R & D CTR
ATTN: CODE 17
2 CYS ATTN: B WHANG
ATTN: CODE 1770
ATTN: CODE 1844

NAVAL FACILITIES ENGINEERING CMD
ATTN: CODE 04B

NAVAL PERS RES & DEV CENTER
ATTN: CODE 71

NAVAL RESEARCH LABORATORY
ATTN: CODE 2627

NAVAL SEA SYSTEMS COMMAND
ATTN: SEA-0351
ATTN: SEA-08
ATTN: SEA-09G53

NAVAL SURFACE WARFARE CENTER
ATTN: CODE R14
ATTN: CODE R15
ATTN: I BLATSTEIN

NAVAL SURFACE WARFARE CENTER
ATTN: TECH LIB & INFO SVCS BR

OFC OF THE DEP CH OF NAVAL OPS
ATTN: OP 03EG
ATTN: OP 981

OFFICE OF NAVAL RESEARCH
ATTN: CODE 1132SM

SPACE & NAVAL WARFARE SYS CMD
ATTN: PME 117-21

DEPARTMENT OF THE AIR FORCE

AFIS/INT
ATTN: INT

AIR FORCE INSTITUTE OF TECH/EN
ATTN: C BRIDGMAN

AIR FORCE SYSTEMS COMMAND
ATTN: DLW

AIR FORCE WEAPONS LABORATORY
ATTN: NTE
ATTN: NTED
ATTN: NTEO
ATTN: NTES
ATTN: SUL

AIR UNIVERSITY LIBRARY
ATTN: AUL-LSE

BALLISTIC MISSILE OFFICE
ATTN: D GAGE

DEPUTY CHIEF OF STAFF/AF-RDQM
ATTN: AF/RDQI

HILL AIR FORCE BASE
ATTN: TRW/H L DEPT

STRATEGIC AIR COMMAND
ATTN: NRI/STINFO

DEPARTMENT OF ENERGY

DEPARTMENT OF ENERGY
ATTN: OMA/DP-225

LAWRENCE LIVERMORE NATIONAL LAB
ATTN: L-53 TECH INFO DEPT LIB

LOS ALAMOS NATIONAL LABORATORY
ATTN: D RICHMOND
ATTN: REPORT LIBRARY

SANDIA NATIONAL LABORATORIES
ATTN: TECH LIB 3141

OTHER GOVERNMENT

CENTRAL INTELLIGENCE AGENCY
ATTN: OSWR/NED

DEPARTMENT OF DEFENSE CONTRACTORS

AEROSPACE CORP
ATTN: LIBRARY ACQUISITION

APPLIED RESEARCH ASSOCIATES, INC
ATTN: N HIGGINS

APPLIED RESEARCH ASSOCIATES, INC
ATTN: J SHINN

APPLIED RESEARCH ASSOCIATES, INC
ATTN: R FRANK

BDM CORP
ATTN: A VITELLO
ATTN: E DOTCHAK

CALIF RESEARCH & TECHNOLOGY, INC
ATTN: K KREYENHAGEN
ATTN: M ROSENBLATT

CALIF RESEARCH & TECHNOLOGY, INC
ATTN: J THOMPSON

CUSHING ASSOCIATES, INC
ATTN: V CUSHING

H-TECH LABS, INC
ATTN: B HARTENBAUM

INSTITUTE FOR DEFENSE ANALYSES
ATTN: CLASSIFIED LIBRARY

KAMAN SCIENCES CORP
ATTN: B KINSLOW

KAMAN SCIENCES CORP
ATTN: E CONRAD

KAMAN SCIENCES CORPORATION
ATTN: DASIAC

KAMAN TEMPO
ATTN: DASIAC

LOCKHEED MSL & SPACE CO, INC
ATTN: J BONIN
ATTN: TECHNICAL LIBRARY

LOCKHEED MSL & SPACE CO, INC
ATTN: S TAIMUTY
ATTN: TECH INFO CTR

MISSION RESEARCH CORPORATION
2 CYS ATTN: B GOPLEN
2 CYS ATTN: J BRANDENBURG
2 CYS ATTN: R WORL

NATIONAL TECHNICAL SYSTEMS
ATTN: P LIBERMANN

PACIFIC-SIERRA RESEARCH CORP
ATTN: H BRODE

R & D ASSOCIATES
ATTN: C K B LEE
ATTN: D SIMONS
ATTN: J LEWIS
ATTN: TECH INFO CENTER

R & D ASSOCIATES
ATTN: C KNOWLES

R & D ASSOCIATES
ATTN: G GANONG

RAND CORP
ATTN: B BENNETT

S-CUBED
ATTN: D GRINE

SCIENCE APPLICATIONS INTL CORP
ATTN: TECHNICAL LIBRARY

SCIENCE APPLICATIONS INTL CORP
ATTN: J COCKAYNE
ATTN: W LAYSON

SOUTHWEST RESEARCH INSTITUTE
ATTN: A WENZEL

SRI INTERNATIONAL
ATTN: J COLTON

TRW INC
ATTN: D BAER
ATTN: TECH INFO CTR

TRW SPACE & DEFENSE SYSTEMS
ATTN: W WAMPLER

WEIDLINGER ASSOC
ATTN: J ISENBERG

WEIDLINGER ASSOC, CONSULTING ENGINEERS
ATTN: M BARON

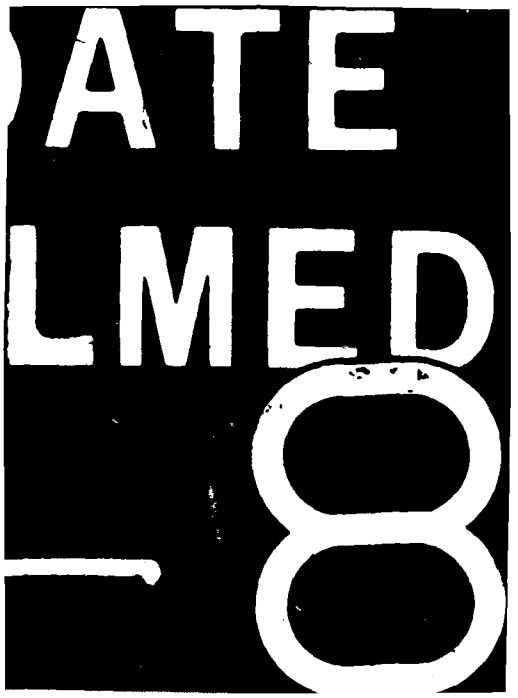
ATE
LMED
8